Development of αFe_2O_3-TiO_2/PPO_{dm} Mixed Matrix Membrane for CO_2/CH_4 Separation

Yun Kee Yap[1], *Pei Ching* Oh[1,*], and *Evan Yew Jin* Chin[1]

[1]CO_2 Research Centre (CO_2RES), Institute of Contaminant Management, Chemical Engineering Department, Universiti Teknologi PETRONAS, 32610 Seri Iskandar, Malaysia.

Abstract. Magnetophoretic dispersion of magnetic fillers has been proven to improve gas separation performances of mixed matrix membrane (MMM). However, the magnetic field induced is usually in a horizontal or vertical direction during membrane casting. Limited study has been conducted on the effects of rotational magnetic field direction towards dispersion of particles. Thus, this work focuses on the rearrangement of paramagnetic iron oxide-titanium dioxide (αFe_2O_3-TiO_2) nanocomposite in poly (2,6-dimethyl-1,4-phenylene oxide) (PPO_{dm}) membrane via rotational magnetic field to investigate the dispersion of filler and effects towards its overall gas separation performance. The paramagnetic fillers were incorporated into polymer via dry phase inversion method at different weight loading. MMM with 3 wt% loading shows the best performance in terms of particle dispersion and gas separation performance. It shows the greatest relative particles count and least agglomerates via OLYMPUS^{TM} Stream software with image taken by optical microscope. Relative to pristine membrane, it displays a permeability and selectivity increment of 312% and 71%. MMM with 3 wt% loading was refabricated in the presence of rotational magnetic field to enhance the dispersion of paramagnetic fillers. Results display an increment of selectivity by 8% and CO_2 permeability by 46% relative to unmagnetised MMM of 3 wt% loading.

1 Introduction

Amidst the ever-increasing human population, the energy consumption has surge to almost twice the median rate for growth in 2010. Fossil energy primarily consisting of coal, gas and natural oil remains the popular choice to fulfil the global energy demand. Among the fossil energies, natural gas accounts for approximately 45% of the rise in combined energy demand for 2018 and is expected to successively overtake coal and petroleum as the main choice of fossil energy consumption worldwide due to its relatively lower pollutant emission rates. However, carbon dioxide present alongside it in gas reservoirs must be extracted due to its acidic and low calorific nature, which would lead to present day problems such as pipeline corrosion and increased transportation cost. Thus, one effective CO_2/CH_4 gas separation method is via mixed matrix membrane (MMM), a combination of homogenously interpenetrating polymeric matrices to ease processability with inorganic particles to produce a membrane that is high in both selectivity and permeability. In most composite material including MMM, the distribution of particles or fillers into the polymeric matrix contributes to the improvement in membrane performance. The filler content and size are tailored to their maximum practical weight loading in order to achieve the ideal MMM performance. Often used size of fillers are in the nano-range due to their high surface area which translates to high energy sites and these features provides strong interfacial interaction in polymer/filler pairings. However, the drawbacks with high surface energy are poor dispersion leading to agglomeration of fillers. These agglomerations form non-selective interfacial voids resulting in higher permeability of gases but lower selectivity. This may be contributed by strong van der Waal forces, high surface energy or hydrogen bonds [1]. Hence, various dispersion methods have been researched extensively in order to reduce the degree of agglomeration. Among the methods were priming of fillers, mechanical dispersion, covalent and non-covalent functionalization, and hybrid. Priming and mechanical dispersion presents itself with drawbacks whereby priming only applicable to low weight loading and the latter causes damage towards particles [2, 3]. As for functionalization and hybrid fillers, various combinations and studies have been conducted to investigate their effects into finding the right match for gas separation performance improvement fillers [4, 5].

Apart from the conventional methods presented, several works have been published regarding the usage of magnetic field to align or disperse the magnetic fillers. It was found that iron-encapsulated carbon nanotubes in poly (2,6-dimethyl-1,4-phenylene oxide) (PPO_{dm}) membrane has ferromagnetic properties and during magnetization whilst casting of membrane, it was claimed that the alignment of filler occurs. As a result, gas separation performance increased after magnetization and

* Corresponding author: peiching.oh@utp.edu.my

with increment of magnetic fillers loading [6]. Hence, there could be a possibility that the magnetic field improved the alignment and dispersion of the filler, thereby contributing to increased separation performance of the MMM [6-9]. It was hypothesized that these magnetic particles created a complex structure in the polymer phase, possibly due to the orientation of magnetic fillers during magnetic casting in the development of MMM [6, 9]. The usage of magnetic composite fillers may be aligned or rearranged in the organic phase of the MMM to improve its gas separation performance. However, limited study has been conducted on the effects of rotational magnetic field direction towards dispersion of particles. Thus, this work focuses on the incorporation and rearrangement of paramagnetic iron oxide-titanium dioxide (αFe_2O_3-TiO_2) nanocomposite in PPO_{dm} membrane via rotational magnetic field to improve the dispersion of filler and enhance its overall gas separation performance. To the best of authors' knowledge, these MMM combination and magnetic field direction application has not been attempted in gas separation MMM development.

2 Materials and Method

2.1. Material

Poly (2,6-dimethyl-1,4-phenylene oxide) (PPO_{dm}) polymer powder, titanium dioxide (TiO_2, >99.5% purity) and 2-propanol (C_2H_6OH, >99.5% purity) were purchased from Sigma Aldrich. Iron (III) chloride hexahydrate ($FeCl_3 \cdot 6H_2O$) and chloroform ($CHCl_3$, > 99.5% purity) were purchased from Merck. Carbon dioxide (CO_2) and methane (CH_4) gases were supplied by Air Products, Malaysia.

2.2. Filler and membrane fabrication

2.2.1 Synthesis of αFe_2O_3-TiO_2 Nanoparticles

Titanium dioxide (TiO_2) was added into a 0.5M Iron (III) chloride hexahydrate ($FeCl_3 \cdot 6H_2O$) solution. The solution is stirred before putting into a hydrothermal autoclave for 5 hours with temperature of 90°C. The slurry was then cooled to room temperature and was transferred to the centrifugal tube. The slurry in the tube was centrifuged thrice with deionized water and 2-propanol. Finally, the slurry was dried in the oven at 60°C for 24 hours and the α-Fe_2O_3-TiO_2 nanoparticle filler was synthesized.

2.2.2 Membrane fabrication

Four membranes of different filler loadings and one of them casted under magnetic field were fabricated via dry phase inversion technique as shown in Table 1. PPO_{dm} and α-Fe_2O_3/TiO_2 filler were dried in an oven for 24 hours to remove moisture. Next, α-$Fe2O_3$-TiO_2 filler respective to PPO_{dm} wt% was added into the chloroform and sonicated for 30 minutes. PPO_{dm} of 22.0 wt% with respect to chloroform was gradually added into the suspension while being stirred for the next 24 hours at 60°C using magnetic stirrer. The dope solution was degassed for 4 hours and left standing overnight at room temperature. The solution was then casted on a clean glass plate at 150µm gap setting and left to dry for 24 hours at room temperature. It was then dried for another 72 hours in the vacuum over at 65°C to remove any residual solvent. As for pristine membrane, there was no addition and sonication of filler into dope solution prior to casting. For MMM being casted under rotational magnetic field, the strength of the field was of 10 Gauss and 32 kHz for a duration of 5 minutes. The rotational direction was generated using a sine wave in an AC circuit and its magnetic strength and frequency was increased gradually till the set value.

2.3 Characterization

The surface and cross-sectional morphology of membranes were analyzed using TM3030 Tabletop Microscope at an accelerating voltage of 15 kV. Membrane was cryogenically frozen in liquid N_2 and fractured into half for cross-sectional analysis. Both morphologies were observed at a magnification of 2000x.

The distribution and dispersion of nanofillers in membrane was examined and analyzed via Optical Microscope (OM, Olympus BX53M) integrated with Olympus Stream and images taken with Olympus LC30 Camera. Five times magnification was set. Filler particles were depicted in red and green colour with green representing agglomeration.

Table 1. Filler Compositions

Sample	Filler wt%	Magnetic Field
MMM-0	0	Absent
MMM-1	1	Absent
MMM-3	3	Absent
MMM-5	5	Absent
MMM-3*	3	Present

2.4 Gas Permeation Test

Gas permeation test was carried out using an in-house built gas permeation rig. Membrane samples were cut into 1.77 cm^2 size and placed between a gas permeation test cell. Pure CO_2 and CH_4 gas test were conducted at a fixed pressure of 3.5 bar and room temperature after equilibrium was reached in the system. The flow rate of permeate was measured using a soap bubble flowmeter. The permeability and selectivity were calculated via equation (1) and (2).

$$\frac{(P)_i}{l} = \frac{Q_i}{\Delta p_i A}\left(\frac{273.15}{T}\right) \quad (1)$$

$$\alpha_{CO_2/CH_4} = \frac{P_{CO_2}}{P_{CH_4}} \quad (2)$$

Where $(P)_i$ is defined as permeability for gas i in Barrer, Q_i is the volumetric flow rate of gas i, Δp is the pressure

difference across membrane, A is the membrane effective surface area, l is the membrane skin thickness. The permeability of the CH_4 and CO_2 are reported in the unit of Barrer (1 Barrer = 1×10- 10 cm^3 (STP).cm/s.cm^2 .cmHg). The selectivity, α, of the membrane for pure gas and negligible downstream pressure are then obtained by dividing permeability of CO_2 over permeability of CH_4.

3 Results and Discussion

3.1 Scanning Electron Microscope

The morphology of the mixed matrix membranes was thoroughly analysed through SEM imaging on their top side and cross-sectional area with a magnification of 2000. All membranes were found to have an average thickness of approximately from 30 to 40 µm. Incorporation of fillers plays a part in increasing the interfacial adhesion between polymer PPO_{dm} membrane and the α-Fe_2O_3.TiO_2 fillers. Densification of macro-sized molecules occurs and causes polymeric phase to experience coiled conformation in its tightest form [10]. Thus, this results in the formation of a thin and dense layered membrane.

Top surface morphology images from Figure 1 illustrates a clear increment of particle and several agglomerations from MMM-0 to MMM-5. However, MMM-3* shows a relatively lesser presence of fillers in comparison to MMM-3. It was deduced that the fillers distanced itself from each other during the application of the magnetic field, causing the observation stated above. Paramagnetic fillers are known to first form a chain-like structure under the presence of a lower strength and frequency of rotational magnetic field. As magnetic actuation torque and fluidic drag torque acting upon the filler reaches an equilibrium, the chain of fillers rotates with a constant angular velocity. The chain of fillers would then separate if the fluidic drag torque surrounding the fillers exceed the magnetic actuation torque, disassembling the structure into several shorter pieces and spreading them further apart [11, 12].

For the cross-sectional SEM imaging in Figure 2, pristine PPO_{dm} membrane shows no apparent defects with a smooth, plain cross-sectional surface. The image obtained can be said that it is dense, non-porous and homogeneous structure. Nonetheless, with the addition of nanoparticle fillers into the polymer matrix, agglomeration become more apparent and visible as the filler loading increases. The agglomeration of nanoparticle fillers was highlighted in red circles with

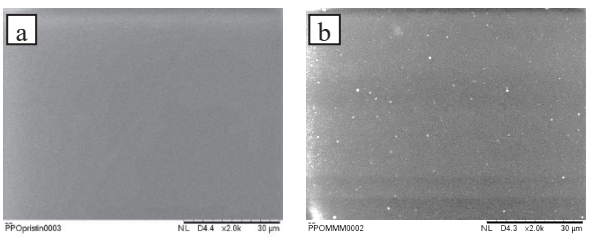

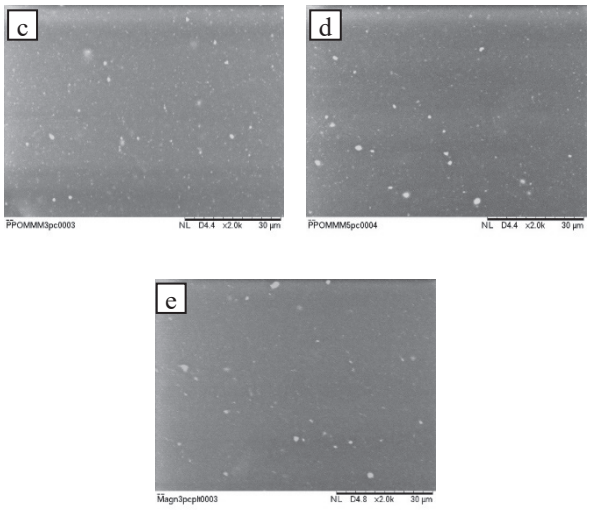

Fig. 1. SEM Imaging of mixed matrix membrane surface morphology (a) MMM-0; (b) MMM-1; (c) MMM-3; (d) MMM-5; (e) MMM-3*

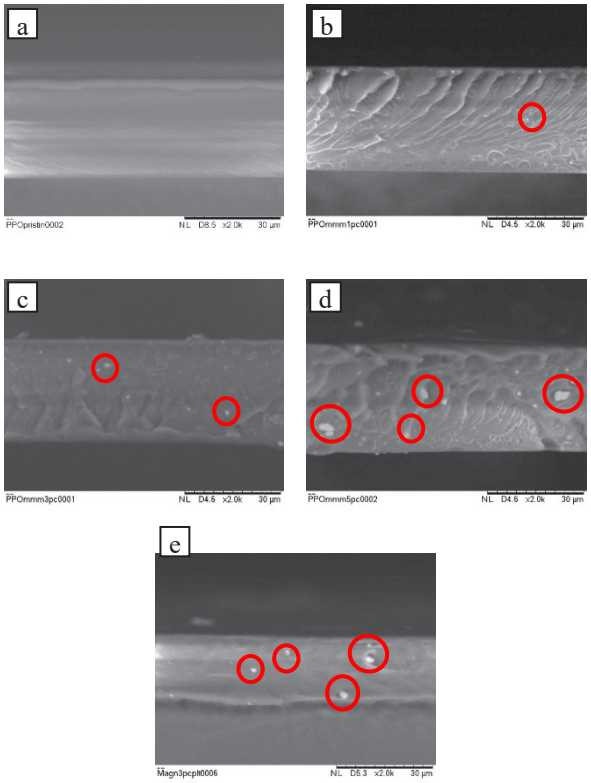

Fig. 2. SEM Imaging of mixed matrix membrane cross-sectional morphology (a) MMM-0; (b) MMM-1; (c) MMM-3; (d) MMM-5; (e) MMM-3*

the most severe belonged to MMM-5. This can be due to the high filler loading which reduces the distance among nano-sized fillers. Nano-sized fillers known for high surface energy that stacks upon each other due to van der Waals forces [13]. Moreover, for the 1.0 wt% and 3.0 wt% fillers, the presence of agglomeration observed but with smaller agglomerate size as compared to 5.0 wt% mixed matrix membrane. The images captured for both top view and cross-section were unbiasedly selected, and all mixed matrix membrane showed the presence of agglomeration,

except for pristine PPO_{dm} membrane. Furthermore, no interfacial voids were observed for all membranes with a wavy-like structure forming around the agglomerates, especially Figure 2 (b) and (d). Overall, the morphology for all mixed matrix membranes remained dense and homogeneous.

3.2 Optical Microscopy

The relative dispersion of paramagnetic fillers in PPO_{dm} polymer matrix was analysed using optical microscope. Figure 3 depicts surface imaging of MMM-1, 3, 5 and 3* with the fillers set to red and green colour. The red colour denotes the size of fillers that are relatively smaller than the larger cluster of fillers represented by the green colour. Based on Figure 3, it can be observed that the amount of fillers in MMM-1 was lesser in comparison to MMM-3, 5, and 3*. Among the latter, it was slightly difficult to discern it qualitatively. The images were then analysed using Stream, an OLYMPUS^{TM} built software to count, measure and classify the particles to its relative sized in each individual image. A fixed threshold was set to classify the size of particles. The images were then classified into two categories which are “dispersion” and “agglomerates”. In Figure 3, dispersion (red colour) represents smaller particle size whereas agglomerates (green colour) represent a larger cluster particle size. The degree of dispersion was analysed in accordance to area fraction and relative object count occupied by both categories of particles and tabulated in Table 2. The area fraction represents the area occupied by the categorized particle, wherein a higher percentage of dispersion signifying a better distribution of small particles throughout the images.

Table 2. Filler dispersion analysis

Sample	Category	Area Fraction (%)	Relative Object Count (%)
MMM-1	Dispersion	36.36	81.69
	Agglomerate	63.64	18.31
MMM-3	Dispersion	38.19	82.31
	Agglomerate	61.81	17.69
MMM-5	Dispersion	34.59	79.73
	Agglomerate	65.41	20.27
MMM-3*	Dispersion	65.85	96.01
	Agglomerate	34.14	3.99

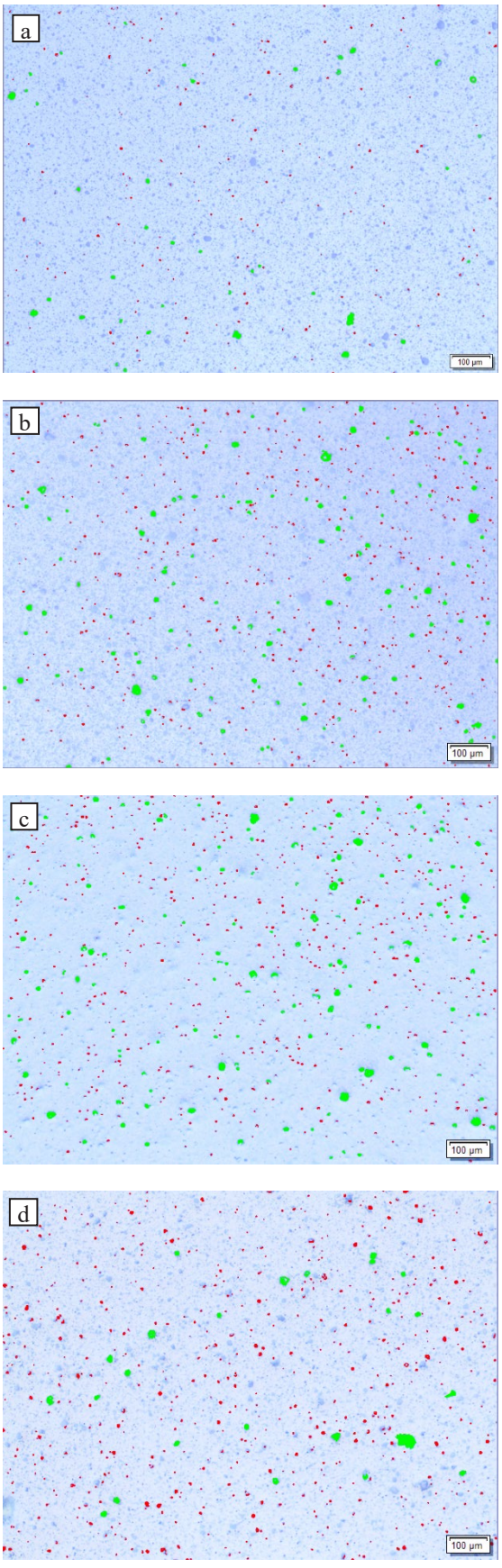

Fig. 3. Optical microscopy of mixed matrix membrane (a) MMM-1; (b) MMM-3; (c) MMM-5; (d) MMM-3*;

The relative object count denotes the amount of individual clustered particles of categorized size in the images. It

does not represent the distribution of fillers throughout the image but rather the amount of categorized particle size present. For MMM-1, approximately 81.69% of fillers were dispersed uniformly. The larger size fillers or agglomeration accounts for 63.64% relative to the area occupied by the fillers. On the other hand, MMM-3 displays a slight increment in dispersion of filler with an 82.31% relative object count of filler present in the image. In addition, there was a slight decrement of area occupied by agglomerates at 61.81%. As filler loading increases, MMM-5 shows the lowest relative object count of filler dispersed at 79.73%, coupled with the highest area occupied by agglomerated filler at 65.85%. It can be noticed that the relative object count of dispersion is higher than agglomerate, which conveys the lower amount of agglomerate relative to finer sized particles. Overall, the values measured signifies that the optimum loading stands at 3 wt% of filler and in agreement with the SEM imaging in previous subsections. As for the final sample, MMM-3* presents a significant increase in dispersion with a relative object count of 96.01%, and a low agglomeration value at 34.14%. This may be attributed to the rotational magnetic field exerted during the casting process, aiding in reducing the clustered particle size and increment in the area occupied by the smaller sized particles.

3.3 Gas permeation test

Pure CO_2 and CH_4 gas permeation test were conducted onto all 5 samples to measure their permeability and selectivity. The results were illustrated in Figure 4 and tabulated in Table 3. A plot of gas permeability against filler weight loading shows that MMM-0 or pristine PPO_{dm} membrane has the lowest pure gas permeability and selectivity of approximately 862 barrer and 1.92. Upon addition of 1.0 wt% filler loading, the permeability of both gases was observed to rise significantly, along with an increment of 38% in selectivity. The presence of small amounts of inorganic fillers disrupts the polymer chain and subsequently leads to increment of free volume within the polymer. This phenomenon then leads to a greater gas diffusion results. However, the studies of iron oxide towards CO_2 affinity has not been extensively studied yet [7]. On the other hand, TiO_2 nanoparticles are also known for its high affinity towards CO_2. Further increase in filler loading resulted in major decrement of gas permeation, especially in MMM-3 and MMM-5. The significant drop in permeability could be due to an increase in agglomeration of fillers in accordance to optical microscopy result. Based on SEM imaging, there seem to be no interfacial voids. Thus, the agglomerates could be deduced to rigidify the polymer chain surrounding it, pointing towards the decrease in gas permeation [14]. Despite the reduction in permeability, the selectivity of both MMM-3 and MMM-5 had an increment of approximately 71% and 9% with respect to pristine PPO_{dm} membrane. The increase in gas permeability in both membranes was followed by an increase in filler loading but higher loading at MMM-5

Table 3. Gas permeation performance of MMM

Sample	P (CO_2)	P (CH_4)	α (CO_2/CH_4)
MMM-0	862.258	448.615	1.922
MMM-1	15033.541	5653.744	2.659
MMM-3	3557.183	1083.084	3.284
MMM-5	2161.910	1030.303	2.098
MMM-3*	5198.038	1463.809	3.551

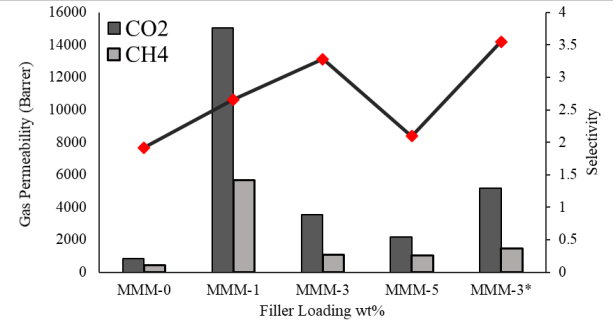

Fig. 4. Mixed matrix membrane gas performance

resulted in the reduction of CO_2 permeability. Thus, the optimal filler loading was observed to be at 3 wt%. The decrease in CO_2 permeability may be attributed to the increase in agglomeration, which possibly reduces the area of contact of αFe_2O_3-TiO_2 filler towards CO_2 molecules. Similar selectivity trend incorporating TiO_2 filler into membrane was observed from Moradihamedani, et al. [15].

The experiment was then repeated with fabrication of MMM with the optimal 3.0 wt% loading under the rotational magnetic field. The resulting gas permeation performance of MMM-3* was then observed to yield an increment of CO_2 permeability of approximately 46% with respect to MMM-3. The selectivity also increased by approximately 8% as well. As mentioned in previous section, the rotational magnetic field could have contributed in improving the dispersion or reducing the cluster size of the filler, which would improve the overall gas separation performance of the MMM. This result in agreement to the optical microscopy wherein a reduction in larger cluster size was measured, along with an increase in finer particle size count. SEM imaging also showed a reduction in larger size particles relative to MMM-3.

4 Conclusion

αFe_2O_3-TiO_2/PPO_{dm} MMM has been fabricated via dry phase inversion at three different weight loadings and the MMM with optimal loading based on best gas separation performance was refabricated in the presence of a rotational magnetic field. The resultant dense MMM showed an improvement of gas permeation performance as compared to pristine PPO_{dm} membrane. MMM casting in the presence of rotational magnetic field for a period of time was observed to enhance the dispersibility of paramagnetic fillers and reduction of filler cluster size. This led to slight improvement of gas separation performance. Therefore, this technique of exposing magnetic fillers under a rotational magnetic field could be

applicable to various magnetic filler and polymer combination.

References

1. R. Atif, F. Inam, Beilstein. J. Nanotechnol., **7**, pp. 1174-1196, (2016)
2. M.R.A. Hamid, H.K. Jeong, Korean. J. Chem. Eng., **35**, no. 8, pp. 1577-1600, (2018)
3. R. Lin, B.V. Hernandez, L. Ge, and Z. Zhu, J. Mater. Chem. A, **6**, no. 2, pp. 293-312, (2018)
4. L. Ge, R. Lin, L. Wang, T.E. Rufford, B. Villacorta, S. Liu, L.X. Liu, Z. Zhu, Sep. Purif. Technol., **173**, pp. 63-71, (2017)
5. S. Saqib, S. Rafiq, M. Chawla, M. Saeed, N. Muhammad, S. Khurram, K. Majeed, A.L. Khan, M. Ghauri, F. Jamil, M. Aslam, Chem. Eng. & Technol., **42**, no. 1, pp. 30-44, (2019)
6. A. Rybak, A. Rybak, W. Kaszuwara, S. Boncel, Diam. Relat. Mater., **83**, pp. 21-29, (2018)
7. H. Riasat Harami, M. Asghari, A. H. Mohammadi, Greenh. Gases., **9**, no. 2, pp. 306-330, (2019)
8. W. Zhu, Y. Qin, Z. Wang, J. Zhang, R. Guo, X. Li, J. Energy. Chem., **31**, pp. 1-10, (2019)
9. A. Rybak, A. Rybak, W. Kaszuwara, M. Nyc, M. Auguścik, Sep. Purif. Technol., **210**, pp. 479-490, (2019)
10. P. S. Murugiah, P. C. Oh, K. K. Lau, Int J Automot. Mech. Eng., **15**, no. 1, pp. 5086-5096, (2018)
11. J. Yu, L. Zhang, IEEE-ASME T. Mech., **24**, no. 1, pp. 154-163, (2019)
12. H. Nakamura, S. Hashi, K. Ishiyama, J. Phys. Conf. Ser., **200**, no. 12, (2010)
13. D.S. Dlamini, B.B. Mamba, J. Li, Sci. Total. Environ., **656**, pp. 723-731, (2019)
14. G.Y.E. Tan, P.C. Oh, K.K. Lau, S.C. Low, Chinese. J. Polym. Sci., **37**, no. 7, pp. 654-663, (2019)
15. P. Moradihamedani, N.A. Ibrahim, W.M.Z. Wan Yunus, N.A. Yusof, Polym. Eng. Sci., **55**, no. 2, pp. 367-374, (2014)